The International Journal of Advanced Manufacturing Technology (2023) 127:5553–5567
https://doi.org/10.1007/s00170-023-11891-3

ORIGINAL ARTICLE

Mechanical properties of 3D-printed staking polypropylene posts for repairing automotive headlights

Fareed Tamaddoni Jahromi[1] · Mostafa Nikzad[1] · Mats Isaksson[1] · Johan Norén[1]

Received: 13 March 2023 / Accepted: 2 July 2023 / Published online: 15 July 2023

Abstract
Additive manufacturing (AM) processes present unique opportunities for the repair of high-value-added industrial and consumer plastic products, which otherwise are destined for the landfill at the end of their life and contribute to the growing environmental and health issues. In this work, we propose a novel method of integrating fused filament-based additive fabrication with the hot staking method to repair a complex automotive component, namely headlight. Newly formulated polypropylene-based composite filaments were used to 3D print a set of staking posts and the missing brackets in the damaged headlight to enable their effective reuse of the repaired assembly. Three staking designs were tested in the first phase of the experiments with the respective geometrical configurations, viz. knurled, domed, and hollow. Strength tests were conducted to rank the performance of the joints against the highest ultimate shear strength values, toughness, and repeatability. The joint design with a domed-shaped profile ranked the best across these criteria. In the second phase of the study, the main printing parameters, including printing temperature, nozzle head penetration in the substrate, printing speed, and layer height, were optimised to increase the joint strength. Based on the design of experiment, the dome-shaped stakes, which were printed using a nozzle temperature of 240 °C, tip penetration of 0.3 mm, 3D printing speed of 12 mm/s, and a layer height of 0.15 mm demonstrated the highest mechanical performance with the bond strength of 7.27 MPa. The repaired headlight was tested under cycling loading showing excellent durability without noticeable degradation of the staked joints upon 10,000 cycles.

Keywords Additive manufacturing · 3D printing · Thermoplastic repair · Staking

1 Introduction

Car accidents can result in expensive repairs for the headlight assemblies. In addition, often a damaged headlight is just replaced, and the broken headlights end up in landfills, adding to the growing environmental and health issues caused by plastic waists, widely reported [1, 2]. One of the common damages to headlight assemblies, even at low-speed collisions or bumps, is the breakage of the headlights' housing lugs (brackets). Repairing a headlight is a manual task that requires highly trained technicians. The process is time-consuming and costly due to the complexity of various lug geometries designed by different car manufacturers. Thus, creating an automated repair method capable of fabricating broken pieces based on their CAD models and joining them to the headlight housing assembly would much improve the conventional repair procedure. Moreover, more complex geometries can be created using this method, enabling the operator to repair a larger range of damaged headlights, and importantly avoiding landfilling of valuable source materials.

In order to identify an appropriate method for repairing plastic headlight lugs, an extensive examination of all the common joining methods for thermoplastics was conducted. Polymeric parts are mainly joined using mechanical fastening, adhesive bonding, and welding techniques. Where necessary, other methods such as hybrid joining (combination of mechanical joining and adhesive bonding) or plastic injection over moulding can be implemented [3]. The adhesion bonding process generally consists of four steps: surface preparation, applying the adhesive, joining the parts under constant pressure, and curing the adhesive. Adhesion bonding is an effective method for joining dissimilar materials using various types of available adhesives that relies on the chemical bonding mechanisms such as the ones found in

✉ Mostafa Nikzad
mnikzad@swin.edu.au

[1] School of Engineering, Swinburne University of Technology, Hawthorn, VIC 3122, Australia

solvent-based systems, aromatic polymers, and thermosetting-based adhesives. This type of joining provides proper sealing on the surface and does not require creating holes in the substrate [4]. However, it has some disadvantageous such as long cycle time, handling hazardous chemicals, generating toxic emissions, complexity for automation, and poor performance on loadings other than shear loading [5]. Mechanical joining methods are relatively fast and simple to apply and can be performed using fastening elements [6] such as rivets, self-tapping screws, or latching mechanisms. They can be used for joining dissimilar materials, while the created joints are easy to disassemble for recycling and do not involve much surface preparation and cleaning steps. However, for repair purposes, they may require creating extra features such as holes for screwing or riveting in the parts, which subsequently can result in structural issues such as stress concentration compromising the integrity of the joints or stress relaxation of materials with viscoelastic nature such as plastics [7].

An analysis of welding techniques available for plastics suggests that several processes can be exploited for joining them based on the joint area, shape, and the number of parts to be joined. Depending on the heat source required for welding, these methods can be classified as conductive, electromagnetic, and frictional welding processes [5]. The main limitations of conductive heating methods, including hot-plate welding and hot-gas welding, are the requirement of surface preparation, exposure of unwanted parts of the headlight to heat, and resultant deformation in the geometry. Welding using electromagnetic heating sources increases the complexity of the automation process as it requires implanting susceptors such as metallic mesh or carbon strip to convert the electromagnetic energy to provide the input energy into material. Additionally, there is a need for controlled environment shielding the joint being developed and hence reducing the possible integrity issues in the joint as well as the safety compliance that may be required due to possible hazzard exposing the users or operators. Lastly, as other conductive components exist in the headlight assembly, microwaves can heat the entire part, which makes this method unsuitable for repair purposes in a robotic cell [8]. Frictional heating source welding methods were also considered not favourable for repair applications. In summary, spin-welding is limited to circular geometries [9], vibration welding [10] suits flat surface shapes, and ultrasonic welding [11] requires a compatible horn for each shape of the repair lug.

Staking is a mechanical joint based on the staking post-deformation using a tool to form a rivet-like mechanical joint. The method can be used for dissimilar materials, is relatively fast, does not require assembly devices and fasteners during the process, does not require adhesives, and can be disassembled for recycling and replacing the joined parts [5]. Moreover, the successful implementation of staking techniques in the automotive industry has been reported in the literature [12]. In the thermal staking process shown in Fig. 1, after assembling the joining components, the staking post is heated above its glass transition temperature using a hot tool. Then, the hot tool and the shaped staking post are cooled down under pressure (Fig. 1b) to form the rivet-like joint. Alternatively, staking can be performed by heating the stake using other heat sources, such as hot air or infrared light, followed by pressing the cold staking tool on the softened plastic to create a rivet. In both cases, the solidification rate can increase by blowing cool air on the staking tool [13].

Abibe et al. [14] studied the mechanical behaviour of staked polymer-metal joints and concluded that the rivet head joint volume and effective cavity filling of the deformed post are the most critical parameters affecting joint strength. As described in ASTM D5961 standard [15], failure in a staked joint may be in the forms of net tension, cleavage, shear-out, and tear-out. In another study by Abibe et al.

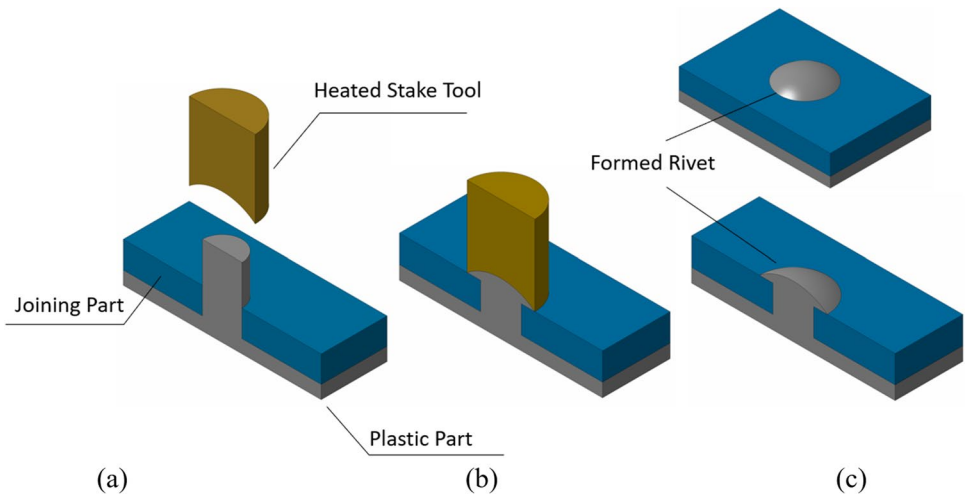

Fig. 1 Schematic of the hot-staking process. **a** Staking tool positioned above the staking post, **b** heated tool is pressed on the post and deforms it, and **c** tool is removed, and rivet is shaped

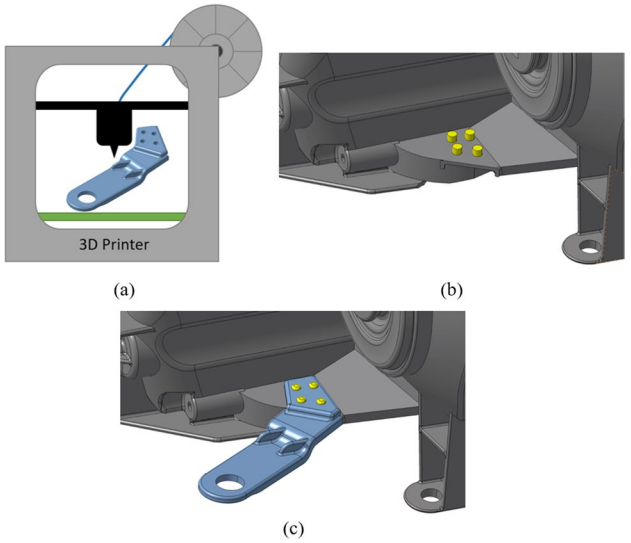

Fig. 2 **a** 3D printing the replacement lug, **b** four stake posts 3D-printed on the damaged headlight assembly, and **c** 3D-printed spare lug staked onto the headlight

[13], a friction-based staking method was compared to an ultrasonic staking method and similar lap shear, and tensile strengths were reported.

Exploring the manufacturing technologies shows that where on-demand, low production volume, high complexity, and customizability are required, additive manufacturing (AM) processes are better suited than their conventional manufacturing counterparts [16–18]. AM techniques have already shown promising results in repairing functional metal parts. Graf et al. [19] utilised the laser metal deposition technique to repair 10 mm deep grooves on stainless steel and titanium alloy specimens. The position control of the specimens and the powder nozzle were performed using a 5-axis CNC machine. Wilson et al. [20] developed a method for repairing turbine blades by laser direct deposition (LDD) technique with a mean accuracy of 0.030 mm. Cold spraying (CS), widely used as a coating method for metals and metal composites, has also been used for repair purposes [21]. For example, repairing the worn surface of an aluminium injection moulding tool [22] and aircraft components made of magnesium and Al–Mg alloy [23, 24] is reported using the CS technique. Several studies in the literature have also reported successful applications of wire arc additive manufacturing (WAAM) for repairing metallic parts such as plain carbon structural steel and grey cast iron [25, 26]. However, applying AM techniques for repairing polymeric structures has received little attention. Recently, we have reported an AM-based approach integrating a new polymer composite formulation coupled with robotic-assisted gripper to enable repairing of an automotive headlight [27].

Among the established AM techniques for processing thermoplastic materials, fused filament fabrication (FFF) and selective laser sintering (SLS) [28], are the two promising candidates to be used in an automated plastic repair system. However, in repair applications where direct 3D printing onto various substrates is required, a powder bed fusion process similar to SLS is not ideal. Relatively speaking, in this context, repairing using SLS would be labour-intensive with higher machine costs and result in waste due to leftover powder feedstock which is difficult to recycle. In contrast, the FFF process is low-cost, generates minimum waste, and can be scaled and automated as assisted by robotic platforms such as the one demonstrated in our recent work. Building upon the joining methods of thermoplastics and the insight derived from the implementation of AM in repair application, we have proposed two novel approaches to repair the headlight housing lugs. In the first method, the broken part is 3D printed directly onto the headlight housing assembly. Whereas in the second approach, the replacement part is 3D printed separately

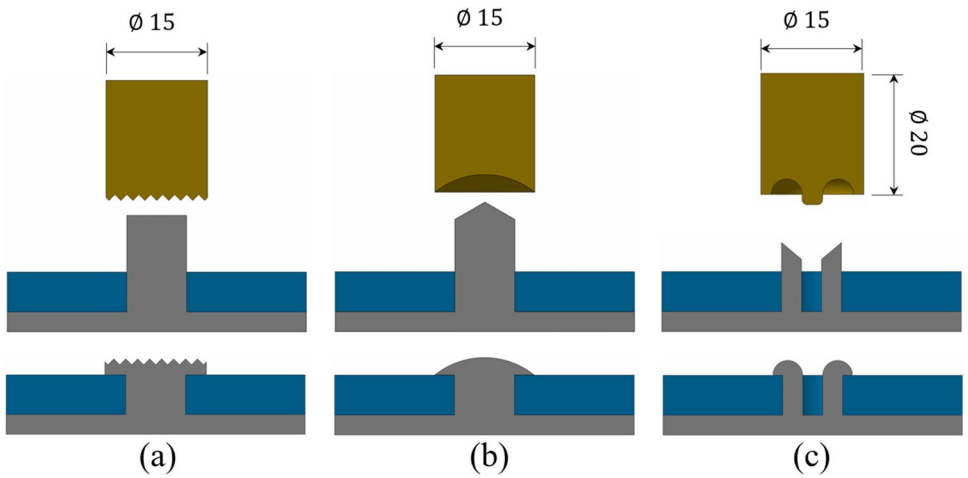

Fig. 3 **a** Knurled, **b** dome, and **c** hollow profiles (dimensions are in mm)

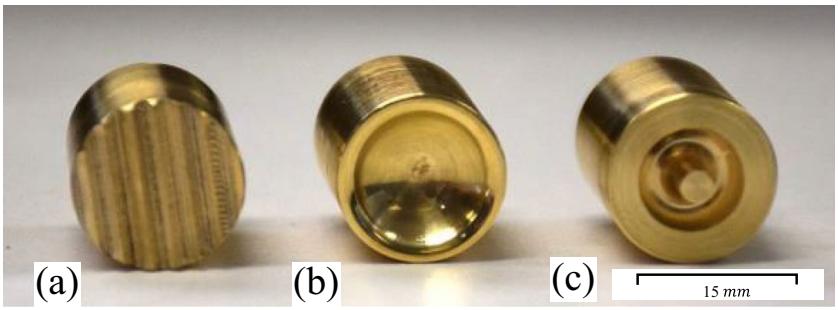

Fig. 4 Brass stake tools for **a** knurled, **b** dome, and **c** hollow profiles

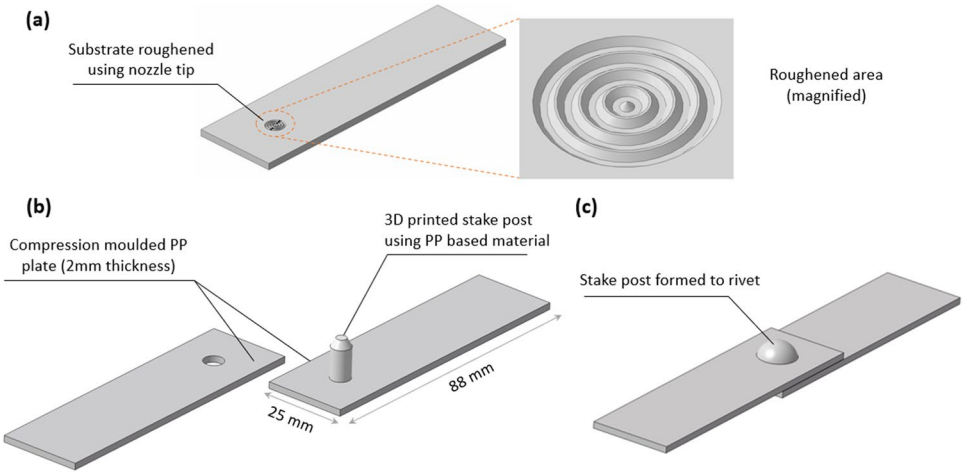

Fig. 5 Schematic of the test specimen preparation for lap shear strength test, **a** roughening the substrate with the 3D printer nozzle, **b** preparing the two joining components, and **c** forming stake joint

using a conventional 3D printer and then attached to the headlight using a hot staking procedure [27]. The first approach eliminates the need for an additional stage of attaching the part to the headlight. However, 3D printing the lug on the headlight surface involves complex synchronisation of the robotic gripping the repairable object and the 3D printing platform, which is yet to be realised. Besides, only a material compatible with the substrate can be used for printing the lugs, limiting the choice of the material. In contrast, the second method allows the lug to be printed using any material and then rely on the specific joining mechanism to achieve the repair outcome.

A schematic of the proposed repair method based on AM and hot staking is shown in Fig. 2. Firstly, the replacement lug is prepared using a 3D printer; at the same time, the staking posts are 3D printed on the headlight housing using a material compatible with the headlight material. Then, the replacement part (shown in blue) is 3D-printed and placed in the proper position by the operator. The 3D-printed staking posts and lug holes are designed so that the lug can fit tightly without clamping. Finally, the staking tool would form the posts to fix the lug in place permanently.

This study explores the parameters of FFF as the material extrusion based additive manufacturing and staking methods to achieve full functional repaired features for an automotive headlight asesmebly. A systematic approach is taken to identify the most suitable staking post design followed by optimising the 3D printing parameters for creating a staking joint with the required mechanical performance.

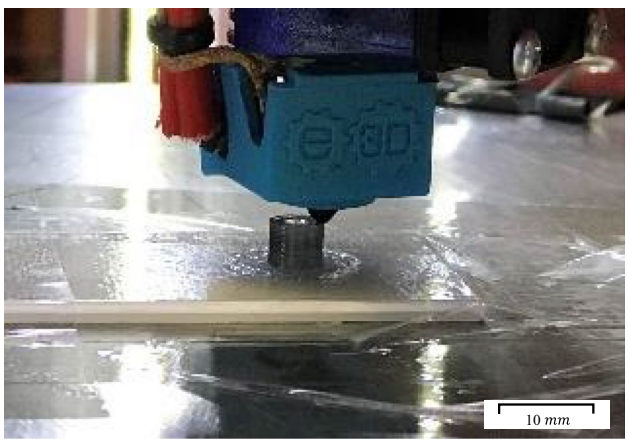

Fig. 6 Hollow profile staking post printed using Tractus3D T850 3D printer

Table 1 Process parameters for 3D printing the staking posts

Parameter	Value
Nozzle temperature	230 °C
Build plate temperature	30 °C
Printing speed	10 mm/s
Penetration in substrate	0.15 mm
Infill type	Concentric
Infill density	100%

2 Materials and methods

2.1 Materials

Headlight housings targeted to be repaired in this project were all made of PP-based materials, according to the original equipment manufacturers (OEM). Therefore, the substrate materials and 3D printing filaments used in this study were PP compounds. Impact copolymer (EP) (Moplen EP548R), manufactured by Al Waha Petrochemical Company, Saudi Arabia, was supplied by LyondellBasell Australia. Verbatim Mitsubishi PP-based 3D printing filament with a fibre diameter of 1.75 mm was supplied by Softdup Pty Ltd, Victoria, Australia, and was used in the experiment's first phase to create the staking posts on EP plate substrates.

In the second part of the experiments, staking posts were created using a newly developed PP-based composite material filament [27]. The material was composed of homopolymer PP, ethylene propylene diene monomer (EPDM), and carbon black (CB) and was extruded into filament with a circular cross-section with a diameter of 2.85 mm. The details of the material preparation and its thermomechanical properties have been described in our previous work [27]. Out of the six different compositions presented in that work, the material composition with 2 wt.% CB inclusion has been used in this research. An Ultimaker 3 FFF 3D printer was implemented for creating the staking posts using the new PP-based material.

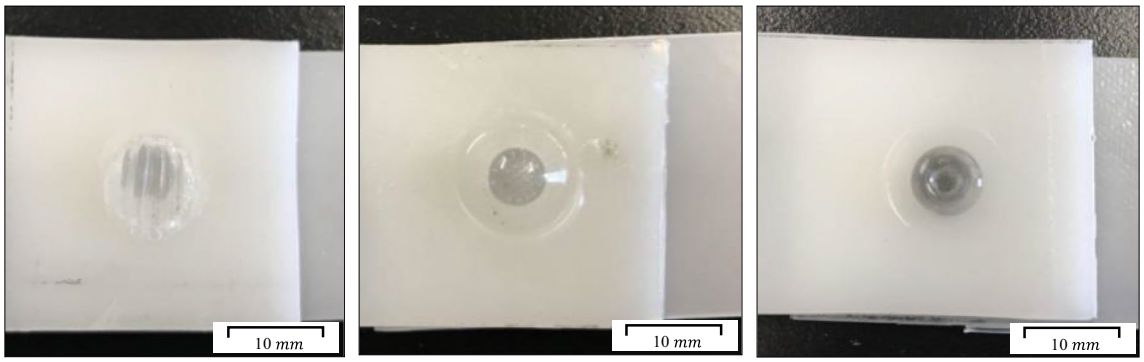

Fig. 7 Stakes created using **a** knurled, **b** dome, and **c** hollow profile

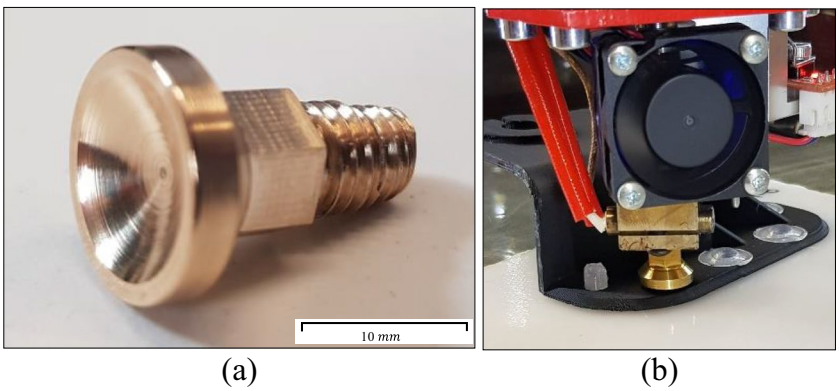

Fig. 8 **a** Modified dome-shaped stake tool with M6 threads. **b** New tool mounted on 3D-printer heat-block

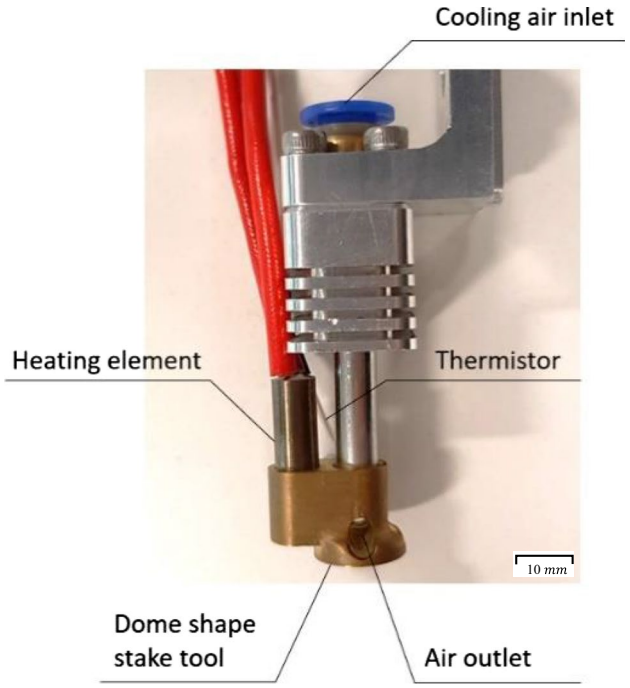

Fig. 9 The final design of the staking tool

2.2 Stake tool design and specimen preparation

Three standard configurations of stake heads were selected to be tested to assess the strength of joints created using the staking method. These configurations included knurled, dome, and hollow cross sections [29] illustrated in Fig. 3. The profiles of staking tools were made of brass to create three different stake types, which are shown in Fig. 4.

Table 2 Key printing parameters selected for stake strength optimisation study

3D-printing parameter	Nozzle penetration (mm)	Nozzle temperature (°C)	Print speed (mm/s)	Layer height (mm)
Value	0	230	8	0.10
	0.15	245	12	0.15
	0.30	260	18	0.20

In order to study the mechanical properties of each stake configuration, samples were prepared according to the ASTM D5961 standard. The polypropylene material was compression moulded into 2 mm thick flat plates. The compression moulded plates were cut into smaller rectangular shapes with the dimensions 88 × 25 × 2mm to be lap joined in pairs using the staking method. The first layer height was set at 0.15 mm deep in the substrate to allow the 3D printer nozzle to roughen the PP plate for better bonding, due to mechanical interlocking between the first 3D-printed layers of the staking post and the substrate. The schematic of the steps for lap joined sample preparation is shown in Fig. 5. The process starts with roughening the PP substrate using the printer head (Fig. 5a) followed by 3D printing a stake post on the roughened area. Afterwards, a 5.5 mm hole, similar diameter to the staking post diameter, was created in another PP plate (Fig. 5b). After assembling two plates, a heat gun set at 400°C was positioned above the staking post at a 50 mm distance, with the nozzle perpendicular to the PP plates. The hot air generated by the heat gun softened the staking post after 10 s. Thereafter, the brass stake head, which was at room temperature (21°C), was pressed on the softened post and remained for 20 s until the post was solidified. Demonstrated in Fig. 6 is the process of 3D printing a

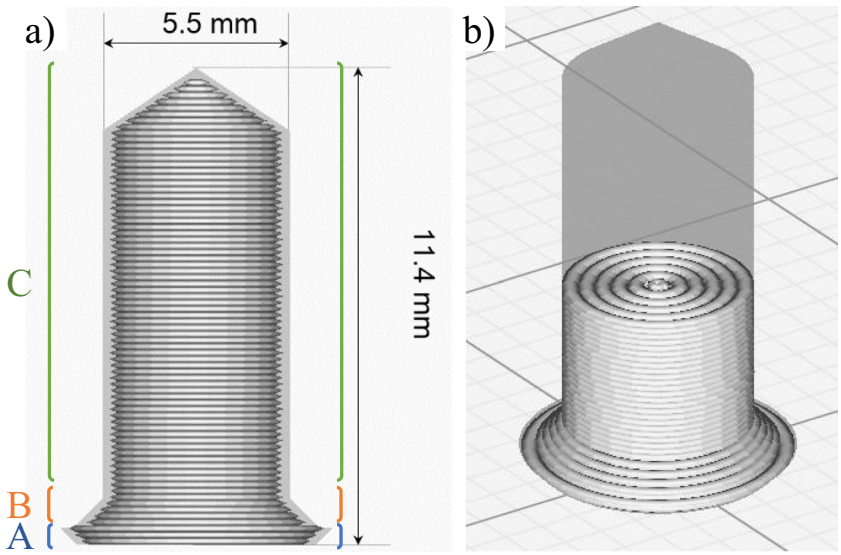

Fig. 10 **a** Final design of the staking post, sliced in Ultimaker; regions A, B, and C are respectively the welding zone, chamfered section, and the body of the stake. **b** Cross-section of the sliced stake model showing the concentric circles for depositing the polymer

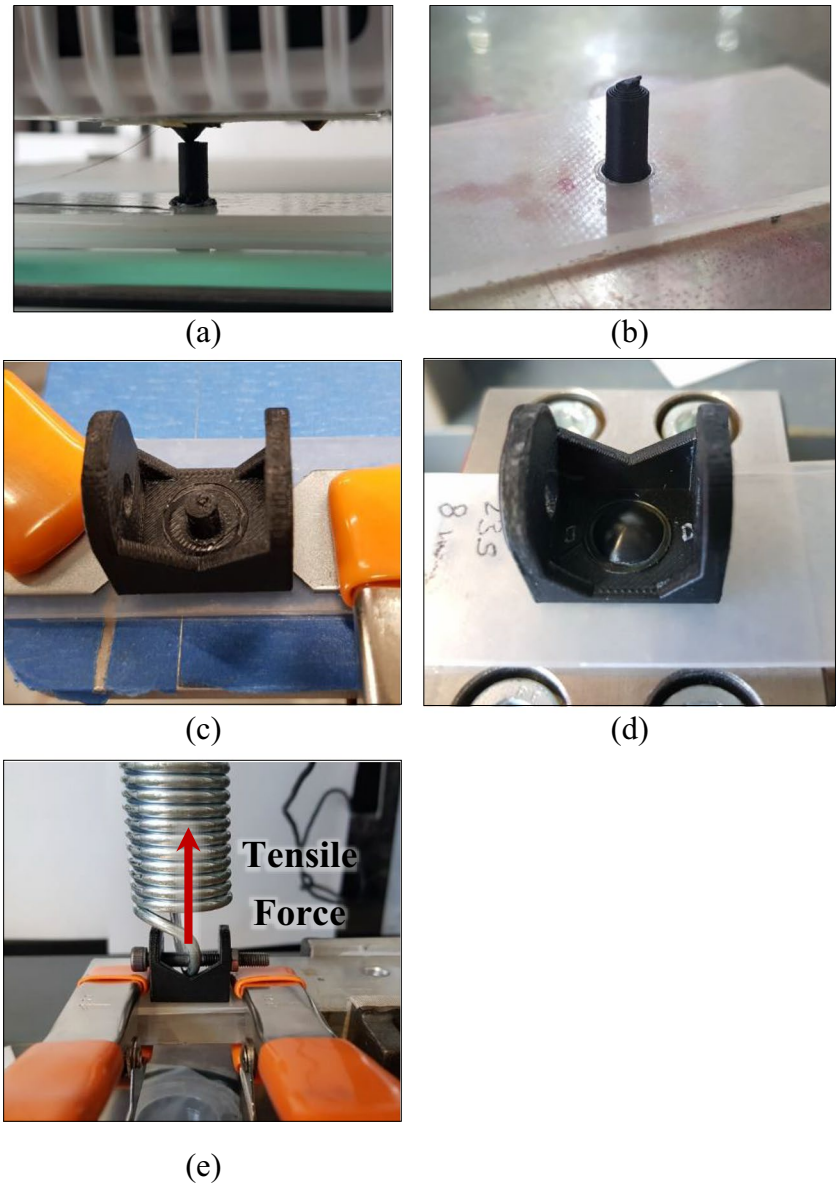

Fig. 11 **a** Printing staking post on PP substrate. **b** Completed staking post on PP plate. **c** ABS bracket assembled on staking post. **d** ABS bracket and PP plate joined using staking. **e** Tensile testing of the joint

staking post using the Verbatim PP material on a PP plate using a Tractus-3D T850 FFF-based 3D printer with a nozzle diameter of 0.4 mm. The printing parameters are summarised in Table 1. Fifteen samples, five from each stake head shape, were prepared using this method. Tests were performed using a Zwick Z010, a universal testing machine (Germany), with a 10 mm/s traverse speed. Bonded samples using different stake tools are illustrated in Fig. 7.

Based on the results obtained in the first series of experiments using three stake head configurations, the dome head stake was selected for the second phase of the experiments. Next, the printing parameters were varied to optimise for a maximum tensile strength in the joints. To facilitate the optimisation process, a new stake head (Fig. 8a) with threads on one side was manufactured and attached to the Tractus-3D T850 3D printer heat block (Fig. 8b) to provide precise control of the tool temperature.

In the new design, a hot stake tool provided the required heat for softening the staking post. However, this increased the cooling time of the staking process. Therefore, the final stake tool (Fig. 9) was equipped with a forced-air cooling mechanism enabling the tool to cool down at a faster rate, which decreased the staking cycle time to 40 s; including 25 s for heating the tool, 5 s of pressing the post and 10 s of cooling.

The final design for the staking post is demonstrated in Fig. 10. As shown in Fig. 10a, the stake deposition is divided into three different regions based on the purpose of each region. The first section, labelled as A, is where the welding

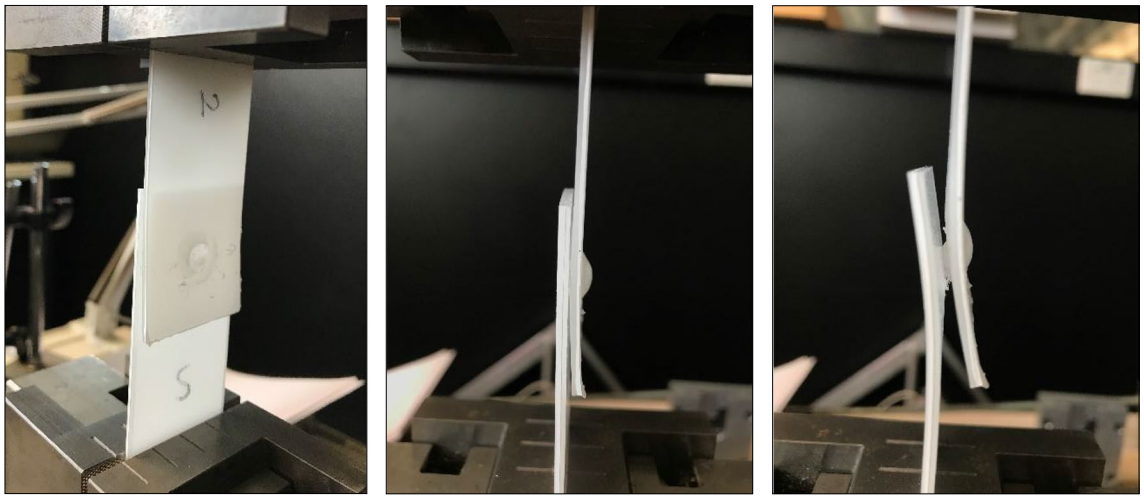

Fig. 12 Dome-shaped stake under shear test. **a** At the start of the test, **b** small deformation after applying the tension, and **c** deformed stake after yield point

happens between the base PP plate and the first layer of the print. To create a strong bond between the base and staking post, at the beginning of the 3D printing process, the printer nozzle penetrates the PP plate to scratch the substrate surface while the printing material is deposited. The roughening step increases the total surface area of the substrate, resulting in a stronger weld between the PP plate and the post. As the 3D printer nozzle tip has a conic shape, a tapered edge is created around the roughened area. Therefore, the base of the designed stake post has the same taper at section A to prevent the creation of a gap between the printed post and the substrate. After depositing two layers in this fashion, the nozzle position is tangent to the PP plate surface, where the printing of section B starts. Section B has a chamfered geometry in order to prevent stress concentration at the stake joint. Finally, the main body of the stake is 3D printed. An Ultimaker[3] 3D printer with a 0.4 mm nozzle was used for printing the samples. Samples were initially created in CAD software and converted to.stl files. Cura 4.3 was used as the slicer software to prepare the g-codes for the 3D printer. Process parameters were defined in Cura to be used for preparing the parts. As demonstrated in Fig. 10b, for all the printed samples, the shell and infill patterns were set to concentric.

In order to optimise the 3D printing process to reach the highest mechanical performance, four parameters, including depth of nozzle penetration into PP substrate (mm), nozzle temperature (°C), printing speed (mm/s), and the layer height (mm), were selected as variables. Table 2 summarises the printing parameters used in this experiment. The analysis started with three different values for nozzle

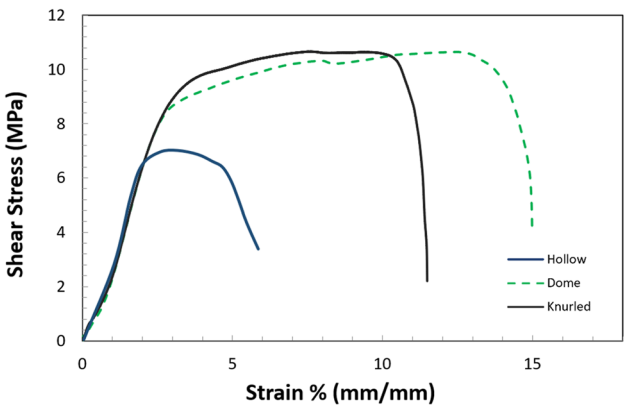

Fig. 13 Shear stress–strain curves for three different stake configurations

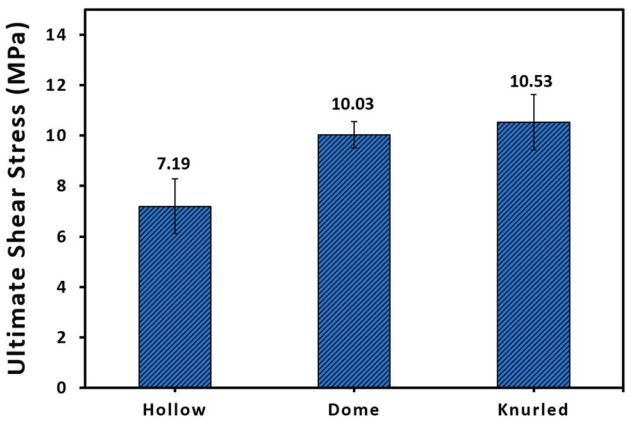

Fig. 14 Average ultimate shear strength of knurled, dome, and hollow stakes

Table 3 Printing parameters for nozzle-penetration-depth sensitivity analysis

3D printing parameter	Nozzle penetration	Nozzle temperature	Print speed	Layer height
Value	0 mm 0.15 mm 0.30 mm	230 °C	12 mm/s	0.15 mm

penetration into the substrate while the rest of the processing parameters were fixed. Once the optimum value for nozzle penetration was found, this value was used as the constant parameter for the next stage in which the nozzle temperature was changing. Likewise, speed optimisation was performed using the optimum nozzle penetration and temperature values. Finally, the effect of layer height was studied once the most acceptable values for the other three variables were found in the previous stages.

Once the staking post was printed on the PP plate substrate (Fig. 11a and b), a bracket made of ABS was assembled on the staking post (Fig. 11c), and the post was formed using the staking tool (Fig. 11d). Finally, the prepared stake joint underwent mechanical testing using the universal testing machine by pulling the bracket in tension while the PP plate was fixed as shown in Fig. 11e. Forces were recorded until the failure of the joint. Throughout this research, a minimum number of three samples were prepared and tested for each set of processing parameters.

3 Results and discussion

3.1 The shear behaviour of different stake shapes under static loading

The mechanical performances of the knurled, dome, and hollow profile stakes were studied using the lap shear test. Through recording the load-deformation graphs, knurled and dome profiles were found to have the highest load value before failure, followed by the hollow-stake profile, which had a weaker performance (Fig. 12). Figure 13 compares the shear stress–strain behaviour of the three different stake shapes, and Fig. 14 presents the average values of the ultimate shear stress of the tested samples.

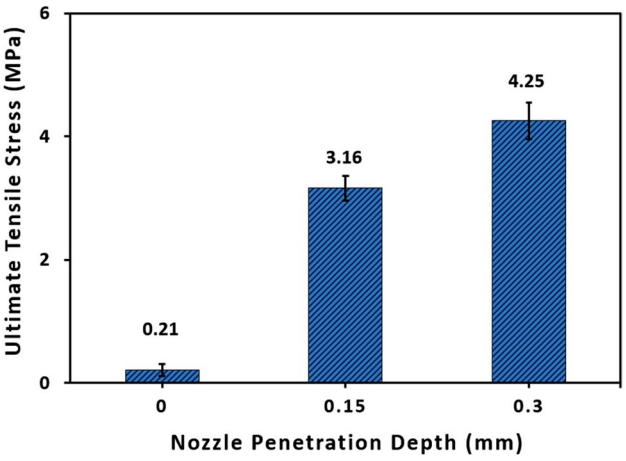

Fig. 16 The effect of nozzle penetration depth in the substrate on the stake mechanical performance

Regarding the similar results for knurled and dome types, other factors were considered for choosing the most suitable stake configuration. Knurled stakes showed high mechanical performance; however, the repeatability and the surface finish were relatively poor. Dome-shaped stakes had appropriate mechanical properties, better repeatability in the results, and the best surface finish. Finally, hollow stakes recorded the lowest mechanical performance but the fastest 3D printing time due to the smaller volume of the staking post. Based on these results, the dome stake was chosen for the final application. Detailed experiments on dome-shaped stakes for optimising the 3D printing parameters are presented in the following sections.

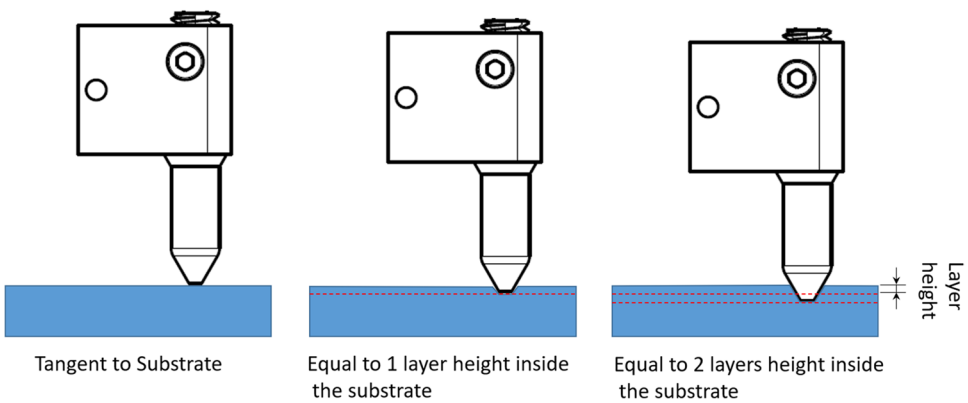

Fig. 15 Variation of nozzle penetration depth

Table 4 Printing parameters for nozzle temperature sensitivity analysis

3D printing parameter	Nozzle penetration	Nozzle temperature	Print speed	Layer height
Value	0.30 mm	230 °C 245 °C 260 °C	12 mm/s	0.15 mm

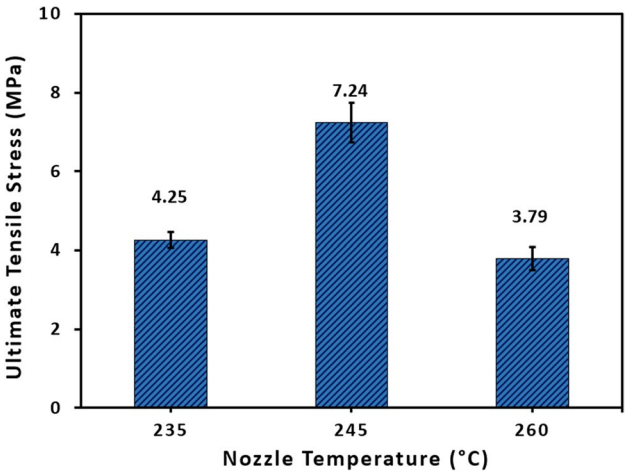

Fig. 17 Nozzle temperature effect on stake mechanical performance

3.2 Effect of 3D-printing parameters on dome stake performance

3.2.1 Effect of nozzle penetration in the substrate

To establish the relationship between nozzle penetration depth in the base material and the strength of the post, they were printed using three different values for nozzle penetration (Table 3). As shown in Fig. 15, the selected depths were 0 mm, 0.15 mm, and 0.3 mm.

For each case, three samples were prepared, and the ultimate tensile strength of all nine samples was measured according to the test procedure previously demonstrated in Fig. 11. The average values presented in Fig. 16 show that starting the first layer print at 0.30 mm inside the substrate leads to the highest mechanical performance. Consequently, the rest of the experiments for finding the optimum printing parameters were performed using 0.30 mm penetration. It should be noted that a higher value for penetration depth, more than 0.3 mm, led to the creation of excess molten plastic from the substrate on the nozzle that interfered with material deposition during the next stages. Moreover, it weakened the 2 mm substrate material as failure in the substrate was observed after the shear test.

3.2.2 Effect of different nozzle temperature

Once the proper nozzle penetration depth was found, different nozzle temperatures were used to understand the effect of deposition temperature on staking performance. The preliminary experiments suggested that weak interlayer bonds are formed between the deposited layers when the nozzle temperature is set below 230 °C. Besides, thermogravimetric analysis (TGA) showed the thermal degradation of the PP-CB-based material at temperatures higher than 260 °C. Therefore, the testing temperatures for this section of the study were selected as 230 °C, 245 °C, and 260 °C. The processing parameters used for 3D printing samples are summarised in Table 4.

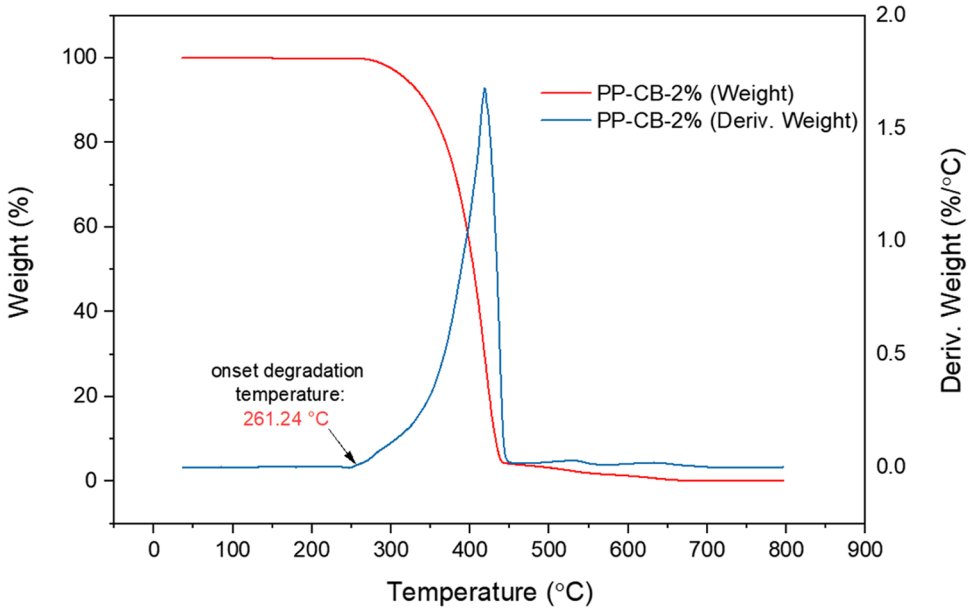

Fig. 18 TGA results of the PP-CB composite filament material

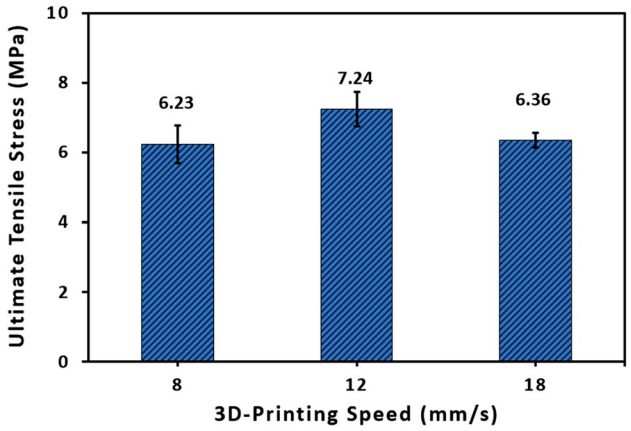

Fig. 19 Variation of stake strength under different print speeds

The test results presented in Fig. 17 show that staking posts created at 245 °C have superior performance under tension. The reduction of staking strength at 260 °C can be explained by the result of polymer degradation at elevated temperatures close to the onset degradation temperature recorded at 261.2 °C using the TGA study (Fig. 18).

3.2.3 Effect of 3D-printing speed

Previous samples were printed at a printing speed of 12 mm/s. Two more speeds, 8 mm/s and 18 mm/s, were tested to understand the impact of the printing speed on the stake's strength. Table 5 summarises the processing parameters utilised for fabricating staking posts.

The results presented in Fig. 19 show that increasing the speed from 8 to 12 mm/s increases the post's strength and decreases again when the printing speed is set to 18 mm/s. However, where higher printing speeds are required for higher productivity, 18 mm/s can be set as the speed, as the drop in the strength is not significant.

3.2.4 Layer height

The last parameter that was studied during the sensitivity tests was layer height. All previous samples were printed using 0.15 mm layer height. In this section, two more layer heights, including 0.10 mm and 0.20 mm, were evaluated (Fig. 20), while the rest of processing parameters remain unchanged as shown in Table 6.

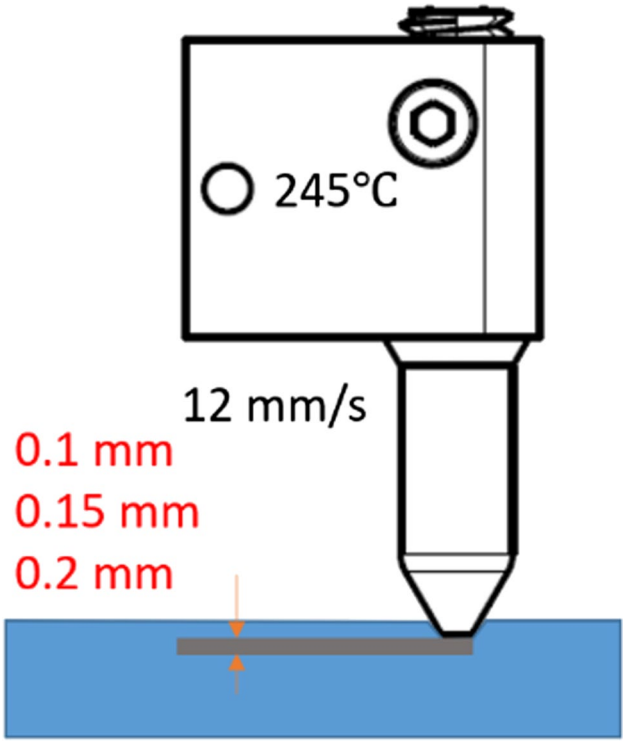

Fig. 20 Variation of layer height

The analysis in Fig. 21 shows that layer heights of 0.1 mm and 0.15 mm provided similar strength, and the strength value dropped by a further increase of 0.05 mm in the layer height. Therefore, 0.15 mm was chosen as the optimal layer height. However, as can be seen in Fig. 21, if in a given print scenario achieving high resolution is essential, the layer height can be set at 0.10 mm with no trade-off in strength. Considering the small amount of strength drop in the 0.20 mm case, this setting can be applied for printing to increase productivity.

Considering that printing at 0.15 mm layer height increases productivity by reducing the 3D printing time, setting the layer height at 0.15 mm is preferred to 0.1 mm. However, depending on the application, when a finer resolution is

Table 5 Printing parameters for printing speed sensitivity analysis

3D printing parameter	Nozzle penetration	Nozzle temperature	Print speed	Layer height
Value	0.30 mm	245 °C	8 mm/s 12 mm/s 18 mm/s	0.15 mm

Table 6 Printing parameters for layer height sensitivity analysis

3D printing parameter	Nozzle penetration	Nozzle temperature	Print speed	Layer height
Value	0.30 mm	245 °C	12 mm/s	0.10 mm 0.15 mm 0.20 mm

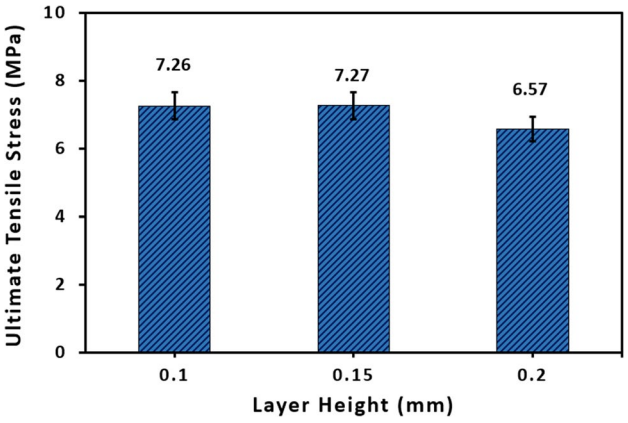

Fig. 21 Stake strength changes for different layer heights

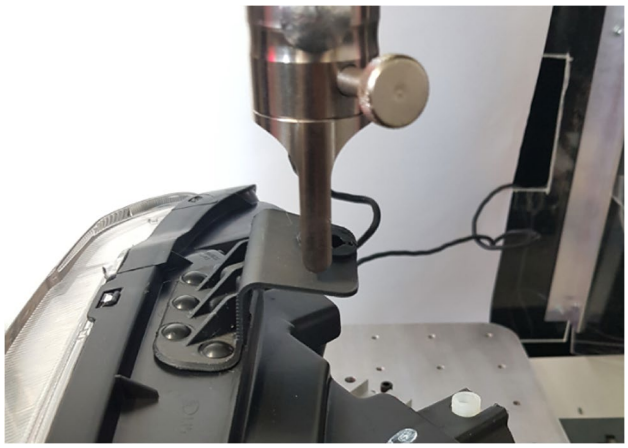

Fig. 22 Set up for cyclic mechanical test applied on the repaired headlight

required, the layer height can be set at 0.1 mm. Although the samples printed at 0.2 mm layer height recorded the lowest strength values, printing at this layer height can increase the printing speed, up to 33% compared to the 0.15 mm case, with only a 10% strength reduction. Therefore, 0.2 mm can still be considered an option for the fabrication of staking posts. Table 7 summarises the steps taken in this research to find the best 3D printing parameters to reach the highest ultimate tensile strength for the 3D-printed staking posts.

The optimised 3D printing parameters were utilised to repair a headlight assembly using the staking method. The repaired lug and the headlight assembly were then subjected to the cyclic mechanical test of 10 N as demonstrated in Fig. 22. After 10,000 cycles, the repaired headlight lug held its integrity and recorded a 1.5 mm deformation in the whole assembly.

3.3 Morphology

An Olympus BX61 Optical Microscope was used to study the print quality and the fracture cross-section area of the samples to ensure that there were no apparent macroscopic defects in the printed joints that could otherwise influence the measured strength data. Figure 23 shows the side view of a defect-free printed stake with 0.1 mm layer height before breakage.

During the test, three mechanisms of failure were observed. The majority of the samples failed at a point close to the stake dome head, followed by the samples that failed close to the PP plate (weld zone) and finally, those failed at a region close to the middle section of the stake. Figure 24 shows the cross-section of three broken samples printed using three different layer heights of 0.1, 0.15, and 0.2 mm. All these samples failed at the top layers near the dome head. The central part of the stakes has experienced a brittle fracture compared to the outer circles that show shear-yielding deformation. This behaviour can be explained by looking at the printing process. During the deposition, the printer nozzle starts by printing the outer wall circle with a larger diameter. As the circles become smaller, the deposition speed of each circle decreases; therefore, the deposited molten polymer has less time to solidify before the adjacent circle is

Table 7 Summary of the variables and the corresponding tensile strength used for the optimisation of the 3D printing parameters for creating staking posts

Variables to optimise the strength of the stakes	Four sets of 3D printing parameters used in this study							
	1		2		3		4	
	Nozzle penetration	Ultimate tensile strength	Nozzle temperature	Ultimate tensile strength	Print Speed	Ultimate tensile strength	Layer Height	Ultimate tensile strength
	0 mm	0.21 MPa	230°C	4.25 MPa	8 mm/s	6.23 MPa	0.10 mm	7.26 MPa
	0.15 mm	3.16 MPa	245°C	7.24 MPa	12 mm/s	7.24 MPa	0.15 mm	7.27 MPa
	0.30 mm	4.25 MPa	260°C	3.79 MPa	18 mm/s	6.36 MPa	0.20 mm	6.57 MPa

Fig. 23 Side view of a 3D-printed staking post with a layer height of 0.1 mm

deposited. Consequently, deposited polymer beads in the core of the stake bond strongly and form a consistent solid with no apparent inner-bead border, so as demonstrated, distinguishing every single bead is impossible.

The second type of failure included those samples that broke at the first layer, where the staking post was welded to the base plate. Marked areas in Fig. 25 show the exposed area of the base PP plate after the sample breakage. It can be seen that a significant amount of the deposited polymer is still bonded to the base. Therefore, it can be concluded that the failure in the first few layers close to the base is due to the stress concentration in that area and not because of the bond breakdown between the staking post and base material.

As observed in Figs. 24 and 25, both brittle and ductile fracture modes are responsible for the stakes' failure. Figure 26 illustrates the difference between the brittle and ductile fracture zones in a sample that has experienced tensile stress. As can be seen, the black area in Fig. 26a is linked to the brittle fracture in the polymer. The magnified area demonstrated in Fig. 26c shows the micro-voids formed during the stake fracture. However, the white-coloured area magnified in Fig. 26b has experienced a ductile fracture where the polymer chains are stretched and microfibrils are formed.

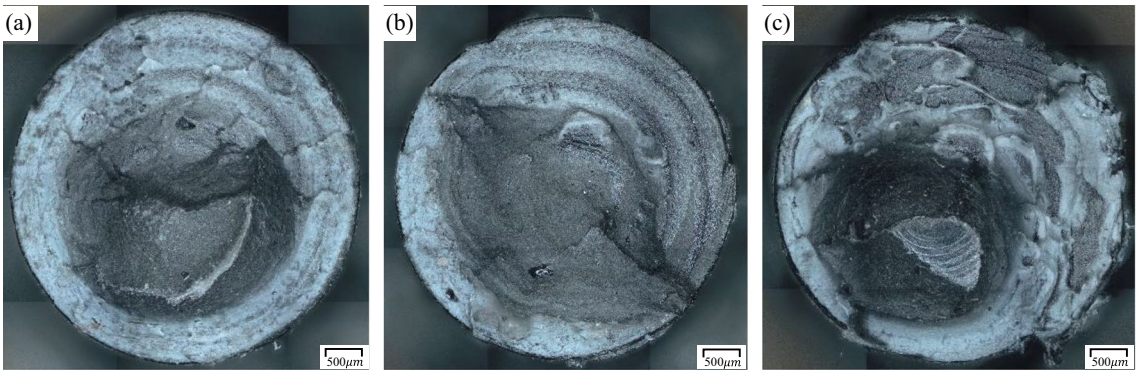

Fig. 24 Fractured surfaces of 3D-printed stakes after breakage with a different layer height of **a** 0.1 mm, **b** 0.15 mm, and **c** 0.2 mm

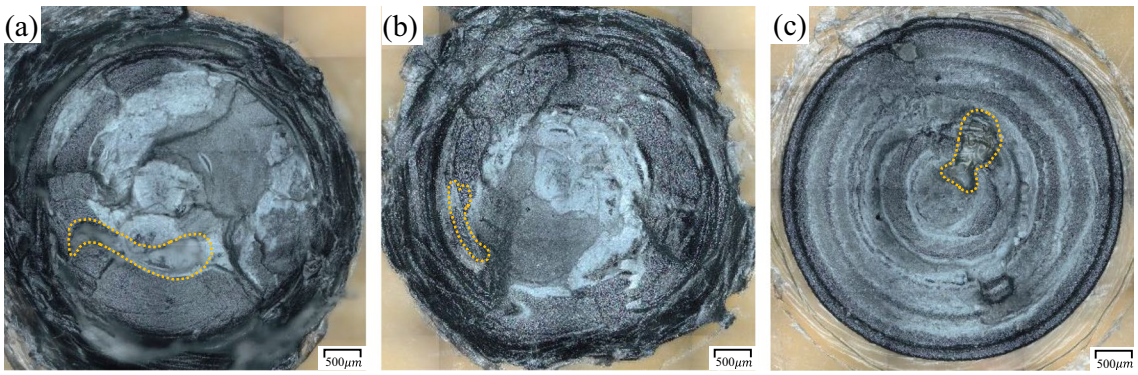

Fig. 25 Fractured surfaces of 3D-printed stakes broken at the stake-PP plate interface. Different layer heights of **a** 0.1 mm, **b** 0.15 mm, and **c** 0.2 mm were set for 3D printing the samples. Annotated using yellow lines are the exposed areas of the substrate material

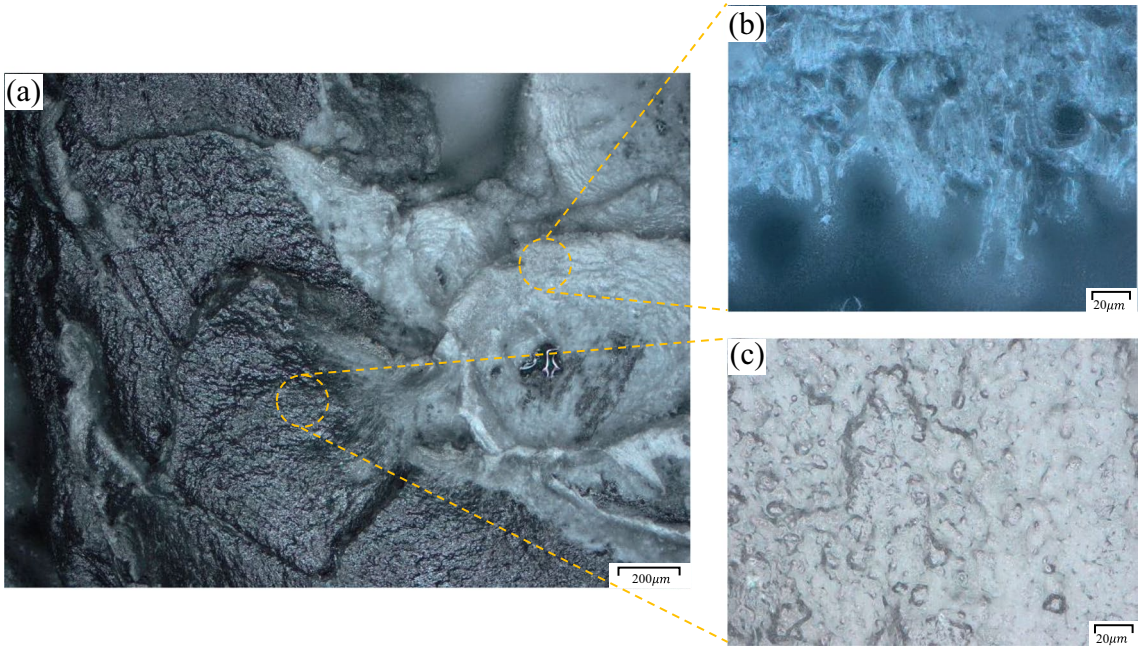

Fig. 26 The fracture surface of a sample with a layer height of 0.1 mm **a** brittle and ductile fractures in the black and white zones, **b** fibrils formed due to crazing, and **c** magnified surface of the brittle fracture

4 Conclusions

This paper proposed staking as a joining method for repairing damaged lugs of car headlights, where staking posts are 3D-printed on the substrate material. Three different stake configurations were proposed, and their mechanical performances were evaluated. The dome-shaped stake was selected for the final stake tool design. Particular attention was paid to the stake tool design and cooling mechanism to decrease the cycle time of creating each stake to 40 s.

The results concluded that it is crucial to initially allow the 3D printer nozzle to penetrate the substrate and roughen it to create a robust mechanical interlocking between the printed post and the PP substrate. It was also shown that under heating and overheating the extruded or base material during 3D printing will reduce the mechanical performance of stakes. The effects of changing the printing speed and layer height in the selected range were not as dramatic as nozzle temperature and penetration depth. Hence, these parameters could be selected in such a way as to ensure a balance between the mechanical performance and the time spent printing a post. The highest strength value for the dome-shaped stake was 7.27 MPa, obtained by setting the nozzle penetration at 0.3 mm, printing temperature at 245 °C, a print speed of 12 mm/s, and a layer height of 0.15 mm. Moreover, the morphology analysis of the stake's fracture surfaces suggests that achieving a better intralayer adhesion between the deposited strands can enhance the overall mechanical performance of the stakes.

Author contribution Fareed Tamaddoni Jahromi: writing — original draft, conceptualisation, investigation, data curation, and visualisation. Mostafa Nikzad: conceptualisation, methodology, software, resources, supervision, and writing — review and editing. Johan Norén: conceptualisation, methodology, and writing — review and editing. Mats Isaksson: conceptualisation, project administration, and writing — review and editing.

Funding Open Access funding enabled and organized by CAUL and its Member Institutions This study was co-funded by the Department of Industry, Science, Energy and Resource (Innovative Manufacturing Cooperative Research Centre) and the Swinburne University of Technology, Melbourne, Australia.

Data availability All data generated in this study are available from the corresponding author upon reasonable request.

Declarations

Consent for publication The manuscript is approved by all authors for publication.

Competing interests The authors declare no competing interests.

References

1. Alabi OA, Ologbonjaye KI, Awosolu O, Alalade OE (2019) Public and environmental health effects of plastic wastes disposal: a review. J Toxicol Risk Assess 5:1–13
2. Verma R, Vinoda KS, Papireddy M, Gowda ANS (2016) Toxic pollutants from plastic waste- a review. Procedia Environ Sci 35:701–708
3. Messler RW (2000) Trends in key joining technologies for the twenty-first century. Assembly Automation 20:118–128
4. Baldan A (2004) Adhesively-bonded joints and repairs in metallic alloys, polymers and composite materials: adhesives, adhesion theories and surface pretreatment. J Mater Sci 39:1–49
5. Amancio-Filho ST, dos Santos JF (2009) Joining of polymers and polymer–metal hybrid structures: recent developments and trends. Polym Eng Sci 49:1461–1476
6. Mori K-I, Bay N, Fratini L, Micari F, Tekkaya AE (2013) Joining by plastic deformation. CIRP Ann 62:673–694
7. Benatar A (2017) 2Applied Plastics Engineering Handbook, In: M. Kutz (Ed.) Applied plastics engineering handbook (second edition), WWilliam Andrew, Oxford, United Kingdom, pp. 575–591
8. Choudhury MR, Debnath K (2019) A review of the research and advances in electromagnetic joining of fiber-reinforced thermoplastic composites. Polym Eng Sci 59:1965–1985
9. Singh R, Kumar R, Feo L, Fraternali F (2016) Friction welding of dissimilar plastic/polymer materials with metal powder reinforcement for engineering applications. Compos Part B: Eng 101:77–86
10. Patham B, Foss PH (2011) Thermoplastic vibration welding: review of process phenomenology and processing–structure–property interrelationships. Polym Eng Sci 51:1–22
11. Benatar A (2015) 12 - Ultrasonic welding of plastics and polymeric composites. In: Gallego-Juárez JA, Graff KF (eds) Power Ultrasonics. Woodhead Publishing, Oxford, pp 295–312
12. Park H-S, Nguyen T-T (2017) Development of a new staking process for an automotive part. Int J Adv Manuf Technol 89:1053–1068
13. Abibe AB, Sônego M, dos Santos JF, Canto LB, Amancio-Filho ST (2016) On the feasibility of a friction-based staking joining method for polymer–metal hybrid structures. Mater Des 92:632–642
14. Abibe AB, Amancio-Filho ST, dos Santos JF, Hage E (2013) Mechanical and failure behaviour of hybrid polymer–metal staked joints. Mater Des 46:338–347
15. ASTM D5961/D5961M-17, Standard Test Method for Bearing Response of Polymer Matrix Composite Laminates, ASTM International 2017
16. Pereira T, Kennedy JV, Potgieter J (2019) A comparison of traditional manufacturing vs additive manufacturing, the best method for the job. Procedia Manuf 30:11–18
17. Sasson A, Johnson JC (2016) The 3D printing order: variability, supercenters and supply chain reconfigurations. Int J Phys Distrib Logist Manag 46:82–94
18. Rodrigues TA, Duarte VR, Miranda RM, Santos TG, Oliveira JP (2021) Ultracold-wire and arc additive manufacturing (UC-WAAM). J Mater Process Technol 296:117196
19. Graf B, Gumenyuk A, Rethmeier M (2012) Laser metal deposition as repair technology for stainless steel and titanium alloys. Phys Procedia 39:376–381
20. Wilson JM, Piya C, Shin YC, Zhao F, Ramani K (2014) Remanufacturing of turbine blades by laser direct deposition with its energy and environmental impact analysis. J Clean Prod 80:170–178
21. Li W, Yang K, Yin S, Yang X, Xu Y, Lupoi R (2018) Solid-state additive manufacturing and repairing by cold spraying: a review. J Mater Sci Technol 34:440–457
22. Lee J, Kang H, Chu W, Ahn S (2007) Repair of damaged mold surface by cold-spray method. CIRP Ann 56:577–580
23. Villafuerte J, Wright D (2010) Practical cold spray success: repair of Al and Mg alloy aircraft components. Adv Mater Process 168:53–55
24. Champagne VK (2008) The repair of magnesium rotorcraft components by cold spray. J Fail Anal Prev 8:164–175
25. Li Y, Han Q, Horváth I, Zhang G (2019) Repairing surface defects of metal parts by groove machining and wire + arc based filling. J Mater Process Technol 274:116268
26. Lee J-H, Lee C-M, Kim D-H (2022) Repair of damaged parts using wire arc additive manufacturing in machine tools. J Market Res 16:13–24
27. Jahromi FT, Nikzad M, Prasad K, Norén J, Isaksson M, Arian A, Sbarski I (2003) Additive manufacturing of polypropylene micro and nano composites through fused filament fabrication for automotive repair applications. Polym Adv Technol 34(2023):1059–1074. https://doi.org/10.1002/pat.5952
28. Ligon SC, Liska R, Stampfl J, Gurr M, Mülhaupt R (2017) Polymers for 3D printing and customized additive manufacturing. Chem Rev 117:10212–10290
29. Rotheiser J (2009) Joining of plastics: handbook for designers and engineers, 3rd edition. ed., Hanser, Hanser Publications, Munich, 2009